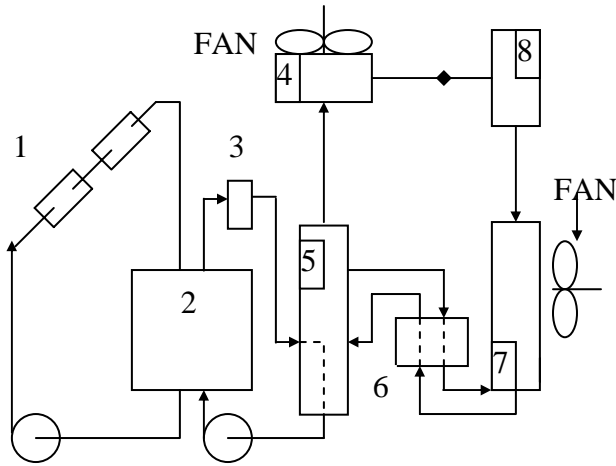


performance of the proposed system as a function of ambient temperature and variable cooling load is obtained through a mathematical and computational simulation.



- (1) solar collectors. (2) storage tank. (3) aux energy source. (4) condenser. (5) generator. (6) heat exchanger. (7) absorber. (8) evaporator.

Figure 2: Air-Cooled Solar absorption System.

The optimal solar energy gain in the collectors is first evaluated by comparing the following options:

- A mass flow rate for the collectors of 0.024 kg/m²s. This mass flow rate was obtained experimentally by González and Khan [3] and is a typical value for forced-circulation systems as specified in the ASHRAE Standard 93 [4].
- Constant temperature increases between input and output of collectors (Melendez [5]).
- Maximum temperature increases between input and output of collectors.
- Maximum useful energy gain from the collectors.

With the optimized collectors, the thermal performance of the proposed system is investigated under dynamic cooling loads that are representative for a small office building in Ponce, Puerto Rico. The cooling loads are calculated using the CLTD method (Krieder & Rabl [6]) and are supplied to the simulation program.

Finally, results are presented for cooling loads of 10.5, 14, and 17.5 kW. For each case, the principal parameters of operation are determined: number of solar collectors, storage tank capacity, operating temperatures for the air-cooled absorption machine, solar collector efficiency, and coefficient of performance (COP).

DESCRIPTION OF AN AIR-COOLED ABSORPTION MACHINE.

Referring to Fig. 2, a diluted lithium bromide solution is created in the absorber. This diluted solution is pumped to the generator, gaining heat as it passes through a liquid-to-liquid heat exchanger. Within the generator, the diluted solution is heated by the hot water supplied from the solar collector loop. A portion of the water is boiled out of solution. The water vapor flows to the condenser, and the resulting, more-concentrated lithium bromide solution flows back to the absorber, losing heat as it passes through the same liquid-to-liquid heat exchanger. The boiled-off vapor is air cooled as it passes through the condenser coil. The two-phase refrigerant is then throttled to a lower pressure and temperature before entering the evaporator. In the evaporator, the refrigerant gains heat from the chilled water loop that provides the space cooling and dehumidification. After leaving the evaporator as a vapor, the refrigerant flows back to the absorber. In the absorber, the concentrated solution from the generator is air-cooled sufficiently enough to cause the refrigerant vapor to be absorbed into solution. The resulting diluted solution is thermally pumped to the generator, thus completing the cycle.

The computer simulation models how heat is removed from the absorber and condenser by air cooling. The heat transfer in the absorber and condenser can significantly influence the performance of the overall absorption cycle. A brief description of the details considered in the simulation for the condenser and the absorber is given below.

Air-cooled Condenser.

The condenser is an air-cooled compact, finned-tube heat exchanger. The type of surface selected is a finned circular tubes, surface 8.0-3/8T (Kays and London [7]), the surface geometric characteristics are:

- Tube outside diameter = 0.0102 m.
- Fin pitch = 315 per meter.
- Flow passage hydraulic diameter = 0.00363 m.
- Fin thickness = 0.00033 m.
- Free-flow area / frontal area, $\sigma = 0.534$
- Heat transfer area / total volume, $\alpha = 179 \text{ m}^2/\text{m}^3$
- Fin area / total area = 0.913 .

The heat transfer from a bank of circular finned tubes in cross flow is considered here and the number of tubes for the heat exchanger is calculated in the simulation program. The finned-tube rows are staggered in the direction of the fluid velocity (see Fig. 3). The superheated vapor comes from the generator into the condenser tubes and is condensed as the heat is removed in the tube bank by the cross-flow air. A similar flow

configuration was proposed by Tongu et al. [2] for their air cooled machine.

The characteristics of the finned-tube heat exchanger are:

- Heat exchanger effectiveness: 0.76
- NTU (Number of Transfer Units): 1.48
- Number of tubes: 150, 175, 199 (for 10.5, 14, and 17.5 kW).
- Outside tube diameter: 0.0102 m.
- Air-side heat transfer coefficient: $0.14 \text{ kW/m}^2\cdot\text{C}$.

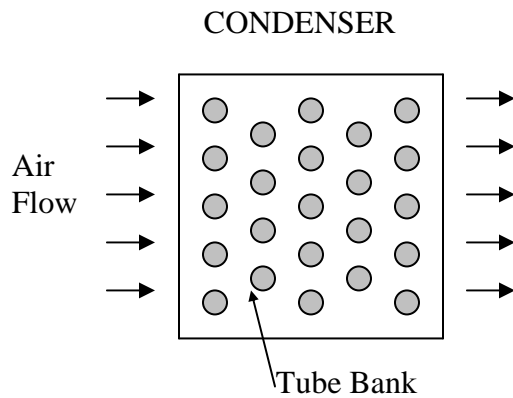


Figure 3: Air-cooled Condenser.

The final dimensions for the condenser were obtained with a simulation code through the Sha's iterative scheme given in Kays and London [7] using constant air temperature increases as controlling variable. This resulted in:

- 0.366m x 0.366m x 0.229m for the 10.5 kW case.
- 0.427m x 0.427m x 0.229m for the 14 kW case.
- 0.488m x 0.488m x 0.229m for the 17.5 kW case.

Air-cooled Absorber.

A similar air-cooled compact, finned-tube heat exchanger used for the condenser is considered here for the absorber with the same finned circular tubes, surface 8.0-3/8T (Kays and London, 1984). The number of tubes for the heat exchanger is calculated in the simulation program in order to satisfy the absorber heat transfer. In this case, the concentrated solution comes into contact with the absorber tubes and is air cooled. Vapor from the evaporator is supplied over the cooled concentrated solution and is eventually absorbed. The resulting dimensions for the absorber were:

- 1.07m x 1.07m x 0.27 for the 10.5 kW case.
- 1.07m x 1.07m x 0.31 for the 14 kW case.
- 1.07m x 1.07m x 0.34 for the 17.5 kW case.

Specific characteristics of the finned-tube heat exchanger are:

- Heat exchanger effectiveness: 0.7
- NTU (Number of Transfer Units): 1.21
- Number of tubes: 524, 582, 640 (for 10.5, 14, and 17.5 kW).
- Outside tube diameter: 0.0102 m.
- Air-side heat transfer coefficient: $0.0516 \text{ kW/m}^2\cdot\text{C}$.

DESCRIPTION OF SIMULATION.

The simulation scheme used here is a modified version of the one presented by Hernández [8]. That simulation is for a coupled system consisting of solar collectors, a non-stratified storage tank and a single effect absorption machine which used a cooling tower for condenser and absorber heat rejection. The refrigerant considered is a lithium bromide – water solution. Modifications made to this prior model included replacing the cooling tower used to remove heat from the condenser and the absorber with air cooling systems and to include optimal flow control strategies in the collectors. In the simulation, the tilted radiation is estimated hourly and monthly for a location in Puerto Rico using the Perez model (Perez et al. [9]). The southern city of Ponce (latitude 18.2° , longitude 67.1°) was considered in the analysis. A variable cooling load for a typical building application is considered for the hours from 8:00 to 17:00. Available data for temperature, the horizontal total radiation, and relative humidity are used (Hernández [8]).

The general sequential steps of the program are presented in Fig. 4.

The input data for the program is:

- Cooling load.
- Location in Puerto Rico.
- Month.
- Load application hours.
- Solar collector characteristics. (Collector size 1.9812 m x 1.2192 m; selective absorber material).
- Solar radiation data.
- Design conditions for the absorber.

The output data is:

- Number of collectors.
- Storage tank volume and temperatures.
- Mass flow rates, temperatures and pressures for the absorption cycle.
- COP.
- Collector efficiency.
- Solar fraction.
- Overall efficiency.

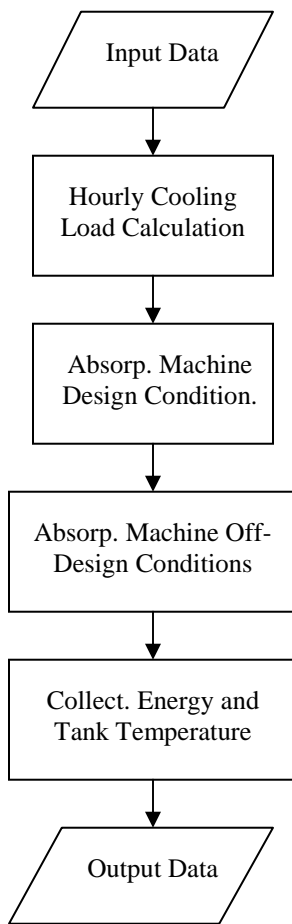


Figure 4: General Program Flow Chart.

RESULTS.

Optimum Energy from the Solar Collectors.

To obtain the largest quantity of energy from the solar collectors, different alternatives were taken into account. The coupled system: collectors – storage tank – absorption machine was considered for the simulation. The alternatives considered were:

- A mass flow rate from the collectors, 0.024 kg/m²s (González and Khan [3]).
- Constant temperature increase between the input and output of the collectors.
- Maximum temperature increase between the input and output of the collectors.
- Maximum useful energy gain from the collectors.

For the first case a mass flow rate for the collectors of 0.024 kg/m²s (González and Khan [3]) was considered, remaining constant for all the operational hours.

The second case considers a fixed temperature increase between the collector inlet and outlet, and a variable collector mass flow rate in the range from 0.01 and 0.09 kg/s. This approach was first suggested by Melendez [5] using a flow range between 0.038 to 0.08 kg/s. The temperature increases considered here were 3 and 4 °C. Increases of less than 3 °C require mass flow rates that are too small at the hours of lowest insolation. For temperature increases of more than 4 °C, smaller quantities of energy are obtained from the collector when compared with the other cases.

For the third case, a maximum temperature increase was obtained between input and output while the collector mass flow rate was made variable. The maximum increase was always obtained with the minimum mass flow rate from the range considered.

In the fourth case, the maximum useful energy gain from the collectors was achieved by varying the collector mass flow rate accordingly.

Higher energy values were obtained for the case of maximum energy gain. The results were higher in 0.8% respect to the 0.024 kg/m² s mass flow rate case, 3% higher respect to the 4°C temperature increase case, 2.3% higher respect to the 3°C temperature increase case, and 8% higher respect to the maximum temperature increase case. The case considering the maximum increase of temperature has the lowest performance, this is due to the fact that higher collectors temperatures increase energy losses.

Figure 5 shows results for the evaluation of the optimum mass flow rate through the collectors. Figure 5 shows results for a typical bank of collectors consisting of 32 collectors. Comparable performance was predicted for the cases of a 0.024 kg/m² s mass flow rate, a 4°C increase, a 3°C increase, and a maximum energy gain.

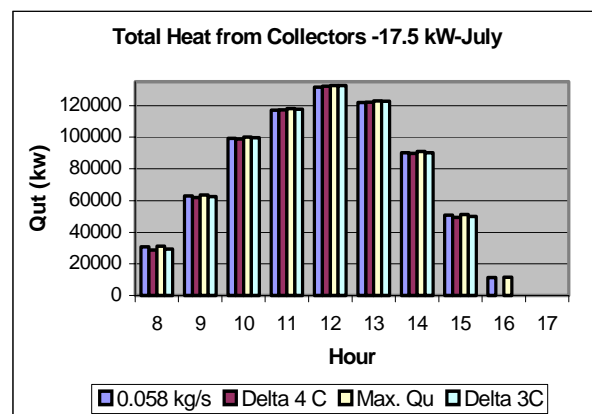


Figure 5: Total Energy from Collectors.

Optimum Solar Collectors and Storage Tank.

The optimum number of collectors for the absorption system to meet was predicted for three dynamic cooling loads using the simulation program. The three cooling loads were based on peak demands of 10.5, 14, and 17.5 kW.

Table 1 shows the mass flow rates and temperature increases for the cases considered. Comparison between cases shows the expected inverse relationship between mass flow rate and temperature rise. For the four best cases, the overall heat transfer, however, is virtually the same.

Hr	Co.MFlowR		Max.DeltaT		DeltaT4C		Max.Qi		Delta3C	
	mc	Del.T	mc	Del.T	mc	Del.T	mc	Del.T	mc	Del.T
	(Kg/s)	(C)	(Kg/s)	(C)	(Kg/s)	(C)	(Kg/s)	(C)	(Kg/s)	(C)
8	0.058	1.1	0.01	5.69	0.015	4	0.09	0.72	0.02	3
9	0.058	2.25	0.01	11.65	0.032	4	0.09	1.46	0.043	3
10	0.058	3.54	0.01	18.39	0.051	4	0.09	2.3	0.069	3
11	0.058	4.18	0.01	22.21	0.061	4	0.09	2.72	0.082	3
12	0.058	4.69	0.01	25.36	0.069	4	0.09	3.05	0.09	3
13	0.058	4.35	0.01	23.88	0.063	4	0.09	2.83	0.085	3
14	0.058	3.22	0.01	17.92	0.047	4	0.09	2.09	0.063	3
15	0.058	1.82	0.01	10.04	0.026	4	0.09	1.18	0.035	3
16	0.058	0.41	0.01	2.22	0.026	4	0.09	0.27	0.035	3
17	0.058	0	0.01	0	0.026	4	0.09	0	0.035	3

Table 1 : Collector Mass Flow Rate and Delta Temp. for : 0.58 kg/s, Max. Temp. Increase, 4°C Increase, Maximum Collector Energy and 3°C Increase.

Table 2 shows the predicted optimum number of collectors for the three cases. The optimum number of collectors is the lowest number of collectors for which a 100 percent solar fraction is achieved at the hour of maximum solar radiation. For the case of Ponce, the hour is 12:00 in the month of July.

k W	O p t i m u m C o l l . N u m .
1 0 . 5	1 9
1 4	2 5
1 7 . 5	3 2

Table 2: Optimum Number of Collectors for Ponce, Puerto Rico (collector area 2.42 m²).

Figure 6 shows the solar fraction vs the number of collectors for the 17.5 kW cooling load case and Ponce location. The optimum number of collectors is predicted

to be 32. Using less collectors is predicted to yield a solar fraction that is less than 100 percent at the hour of maximum radiation. Using more collectors than 32 does not make a higher solar fraction at the hour of maximum radiation. The design thus would be oversized.

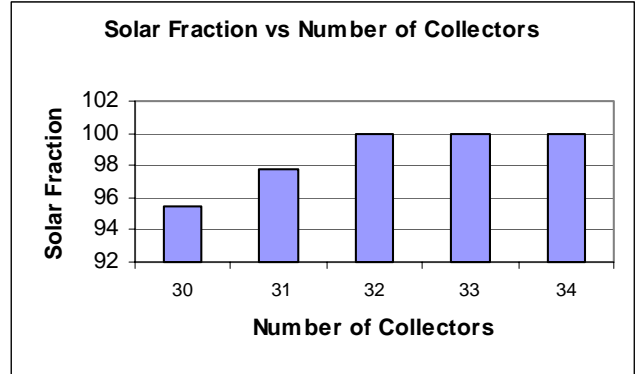


Figure 6: Solar Fraction vs Collector Number for the hour of maximum solar radiation in Ponce, and for the 17.5 kW cooling case.

The storage volume is calculated as a function of the optimum number of collectors. The optimum storage volume to collector area ratio for a static cooling load condition was reported by Hernández [8]. The reported value was 40.5 l/m². For a dynamic cooling load, higher values for the storage volume to collector area ratio were predicted to be needed to maximize the annual solar fraction, Fig. 7. The higher values obtained under a dynamic cooling load can be explained as being due to the delay in the peak loading. In the dynamic case, a smaller cooling load is reflected at the hours of maximum solar radiation. More energy storage is needed to compensate in the peak cooling load occurring at a time when the solar radiation is decreasing. Therefore, a higher storage tank volume is required. The value of 125 l/m² is projected as the optimum value for the 10.5, 14, and 17.5 kW cases.

Figure 8 shows the collector efficiency, COP, and solar fraction for the air-cooled absorption system when subject to a dynamic cooling load. Similar results were found for the 10.5, 14, and 17.5 kW cases. The solar fraction expresses the contribution of the solar energy to the total load in terms of the fractional reduction in the amount of extra energy that must be supplied. The COP is given by:

$$COP = \frac{\dot{Q}_{evap}}{\dot{Q}_{gen}}$$

where \dot{Q}_{evap} is the heat removal rate at evaporator in kW, and \dot{Q}_{gen} is the heat supply rate to generator in kW.

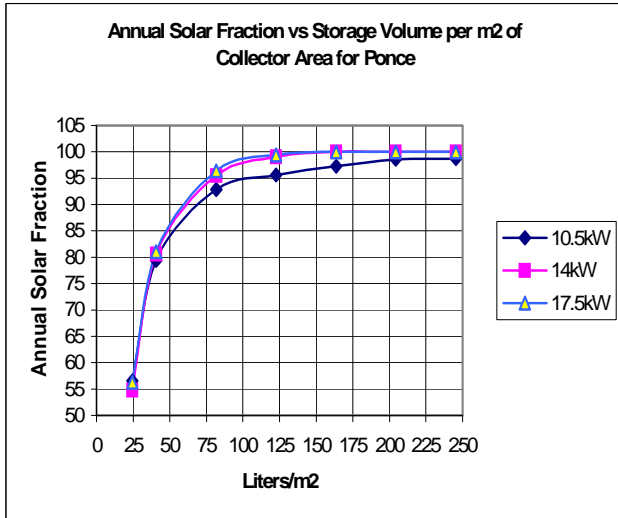


Figure 7: Annual solar fraction vs storage volume per collector area ratio, for location Ponce and dynamic cooling load.

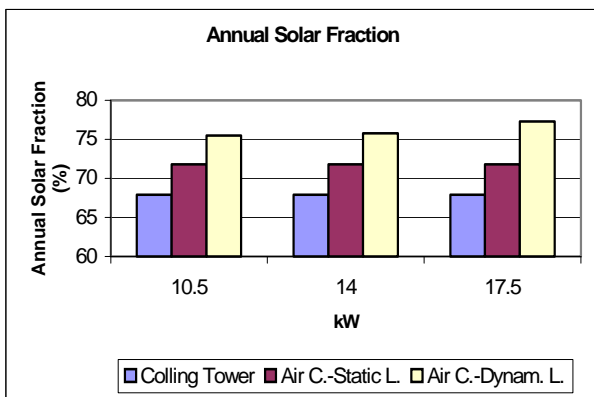


Figure 8: Annual Solar Fraction.

Results of collector efficiency, COP and solar fraction for the case of using a cooling tower are shown in Fig. 9. Similar values were found for the 10.5, 14, and 17.5 kW cases.

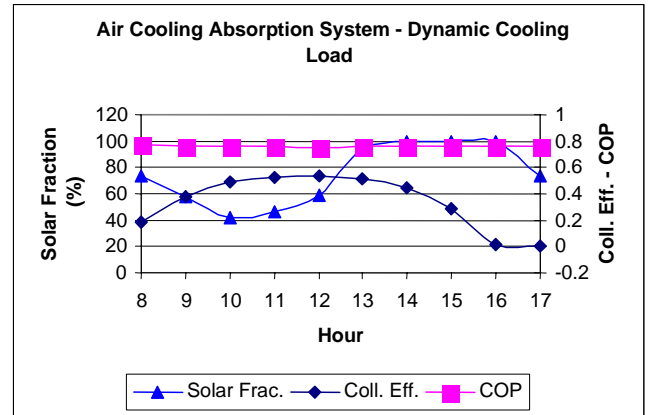


Figure 9: Hourly solar fraction, COP and coll. efficiency– Month: July – Location Ponce, air cooling absorption system under dynamic cooling load.

A comparison between both cases, water and air cooled, indicates that annual solar fractions for Ponce were found to be 67.9% for the case of water cooling (cooling tower), 71.8% for the case of air cooling and a static cooling load, and around 76% for air cooling and a dynamic cooling load as shown in Fig. 8. As can be seen from Fig. 9 and 10, values for COP looks similar, however there are some differences. The solar fraction is higher for the case of air-cooling and dynamic cooling load because the peak load is delayed. The lowest values for the collector efficiency are for the cooling tower case due to the lack of phase between cooling load and solar radiation.

Similar results were found for the 10.5, 14, and 17.5 kW cases, so the annual solar fraction is almost constant when considered as a function of the cooling load.

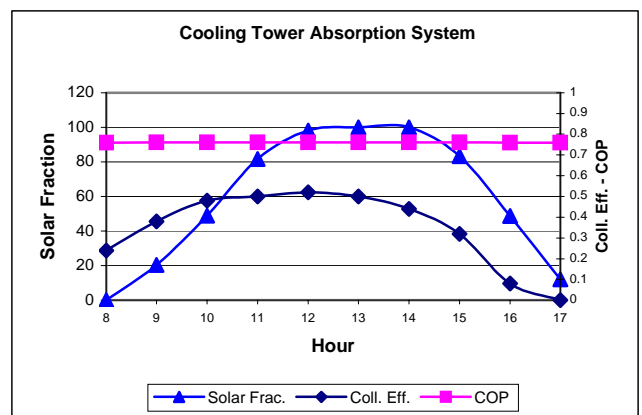


Figure 10: Hourly solar fraction, COP and coll. efficiency– Month July – Location Ponce, for cooling tower under static cooling load.

Finally, the overall efficiency is calculated using the relationship suggested by Meza et al. (1998):

$$\eta_{oe} = \frac{Q_e}{IT * A_c} * 100$$

where:

- Q_e : evaporator heat in kJ/hr.
- IT : hourly total radiation in kJ/hr*m².
- A_c : total collector area in m².

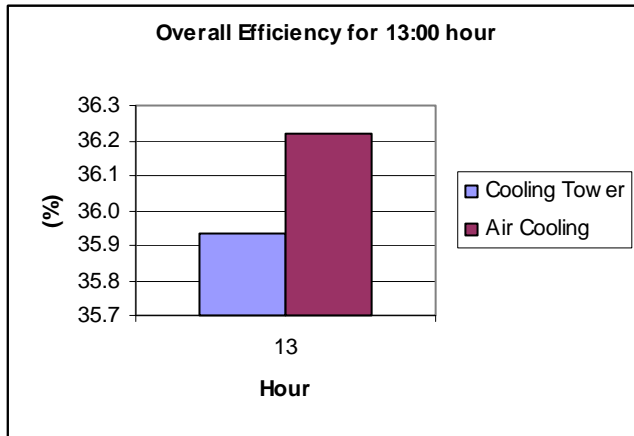


Figure 11: Hourly overall efficiency.

In practical terms Q_e is the useful cooling of the conditioned space. The overall efficiency for the hour of maximum solar radiation (13:00 for Ponce) for the case of air cooling and water cooling (cooling tower) is shown in Fig. 11. As can be seen, values are almost the same for both cases. Similar results were found for the 10.5, 14, and 17.5 kW cases.

Thermal Performance of the Absorption Machine.

The thermal performance of the proposed air-cooled absorption machine was investigated in further detail and similar results were found for all three cases. Results are provided in Fig. 12 and 13. Hourly results are obtained in the simulation program for the thermodynamic cycle of the absorber.

Figure 12 shows the condenser and absorber temperature for air cooling and water cooling absorption machines and the ambient temperature for the working hour cycle from 8:00 to 17:00. While the water cooling values are steady the air-cooling values change as the air temperature changes. Some difference is noted during the early and late hours respect to the water cooling values. Figure 13 shows values for the generator temperature for air cooling and water cooling. Similar trends are noted

between the cases in study. Figure 14 shows the condenser pressure for air cooling and water cooling. In general, higher values for the case of air cooling with respect to the water cooling case were found.

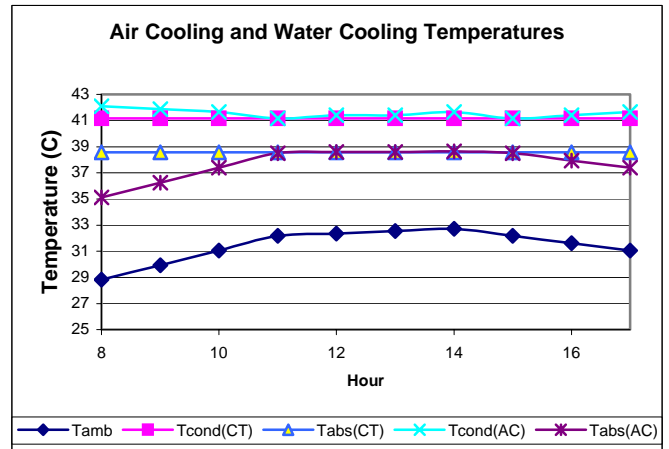


Figure 12: Absorption Cycle Temperatures for Air Cooling and Water Cooling.

Figure 15 shows the COP vs ambient temperature for the air cooling absorption system. As can be noted the COP decreases as the ambient temperature increases.

Figure 16 shows the COP for air cooling and water cooling, and some higher value is noted for the case of air cooling in the earlier and later hours with respect to water cooling. From 11:00 to 15:00 the air cooling COP decreases due to the increase in the ambient temperature, while the cooling tower one keeps almost constant.

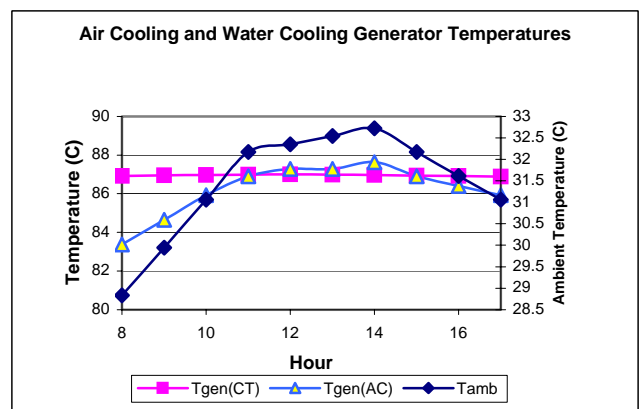


Figure 13: Generator Temperatures.

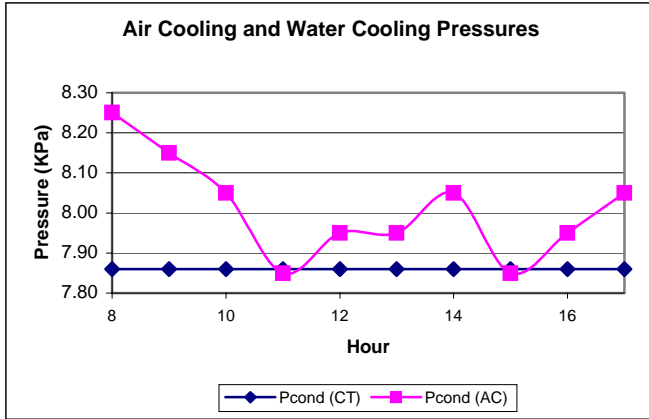


Figure 14: Condenser Pressure.

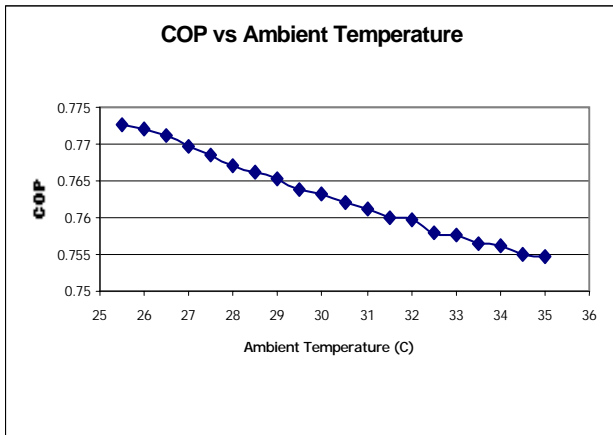


Figure 15: COP vs ambient temperature for air cooling.

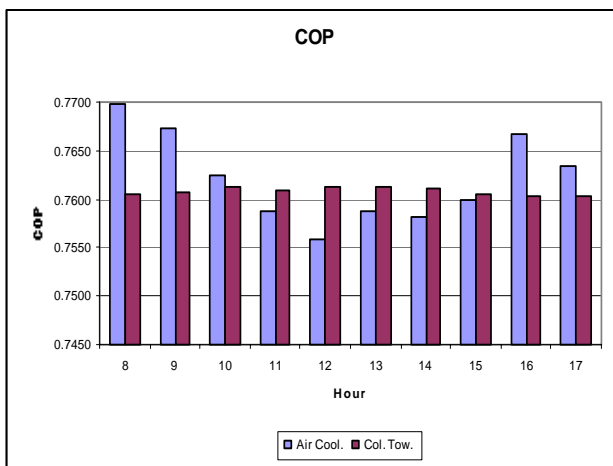


Figure 16: COP of the Absorption Cycle.

CONCLUSIONS.

This paper presents simulation results for the thermal performance for a conceptual air cooled absorption air conditioning system. Air cooled absorption machines could have the great advantage of reducing maintenance and cost when compared with conventional water cooled ones for small cooling loads. The present paper focused in dynamic cooling loads in the range of 10.5, 14, and 17.5 kW.

It was found that the maximum quantities of energy gained by the solar collectors were obtained when using the maximum useful energy gain as control variable when compared with three other operational modes. The constant collector mass flow rate case obtained values only 0.8% lower respect to the maximum useful energy gain case. The other two cases showed larger differences when compared with the case of maximum useful energy gain.

The optimum value found for the storage volume to collector area ratio for a dynamic cooling load was achieved is 125 liter/m². This value is higher respect to the 40.5 liter/m² value for static cooling load reported by Hernández [8].

Very similar results were found for the collector efficiency, the solar fraction and COP for air cooling and water cooling cases especially at the hours with maximum solar radiation for working hours from 8:00 to 17:00.

The results for the thermodynamic properties for the air-cooled absorption cycle are very close to those for the absorption cycle with cooling tower, specially at the hours of higher solar radiation. Similar trends were found for 10.5, 14, and 17.5 kW cases.

The COP for the air cooled absorption machine decreases as the ambient temperature increases.

ACKNOWLEDGMENTS.

This work was partially supported by the National Science Foundation under grant number STTR 9960710.

REFERENCES.

- [1] Meza J.I., A. Y. Khan, and J. E. González, 1998, "Experimental assessment of a solar-assisted air conditioning system for applications in the Caribbean", Proceedings of the Solar Engineering 1998 Conference, pp. 149-154, New Mexico.
- [2] Tongu S., Y. Makino, K. Ohnishi, and S. Nakatsugawa, 1993, "Practical operating of small-sized air-cooled double effect absorption chiller-heater by using lithium bromide and aqueous",

- International Heat Pump Conference, ASME, AES-Vol. 31.
- [3] González, J. E. and A. Y. Khan, “Solar-Assisted Air Conditioning System for Applications in Puerto Rico”, Final Report 96-311 of the Urban Consortium Energy Task Force.
- [4] ASHRAE 93-1986, “Methods of testing to determine the thermal performance of solar collectors”, American Society of Heating Ventilating and Air Conditioning Engineers, Atlanta, Georgia.
- [5] Meléndez L, 2000, “Automation and Control of Solar Air Conditioning Systems”, M.S. Thesis, University of Puerto Rico – Mayagüez.
- [6] Kreider J. and A. Rabl, 1994, “Heating and Cooling of Buildings”, McGraw-Hill.
- [7] Kays W.M. and London, A.L., 1984, “Compact Heat Exchangers”, third Ed. McGraw-Hill Book Company. New York.
- [8] Hernández H., 1997, “Analysis and Modeling of a Solar-Assisted Air Conditioning and Dehumidification System for Applications in Puerto Rico”, M.S. Thesis, University of Puerto Rico – Mayagüez.
- [9] Pérez R. R., R. Seals, P. Ineichen, R. Stewart, and D. Menicucci, 1987, “A new simplified version of the Perez Diffuse Irradiance Model for tilted surfaces”, Solar Energy, Vol.39, pp. 221-231.
- [10] ASHRAE, 1993 ASHRAE Handbook – Fundamentals, American Society of Heating Ventilating and Air Conditioning Engineers, Atlanta, Georgia.
- [11] Hernández H., J.E. González, and A.Y. Khan, 1997, “A parametric study of solar assisted air conditioning and dehumidification systems operating in the Caribbean region”, Proceedings of the Solar Engineering 1997 Conference, pp. 327-333, Washington, D.C.